Desalination and Water Treatment
www.deswater.com

doi: 10.5004/dwt.2017.20464

67 (2017) 187–195
March

Development of iron oxide nanoparticle adsorbents for arsenic and fluoride removal

Prathna TC[a,*], Saroj Kumar Sharma[a], Maria Kennedy[a,b]

[a]*Environmental Engineering and Water Technology Department, UNESCO-IHE Institute for Water Education, 2601 DA, Delft, The Netherlands, emails: p.thanjavur@unesco-ihe.org (Prathna TC), s.sharma@unesco-ihe.org (S.R. Sharma)*
[b]*Faculty of Civil Engineering, Delft University of Technology, Stevinweg 1, 2628 CN, Delft, The Netherlands, email: m.kennedy@unesco-ihe.org*

Received 5 October 2016; Accepted 24 December 2016

ABSTRACT

The study was designed to synthesize iron oxide nanoparticles and to investigate their application as a sorbent to remove fluoride and arsenic from contaminated water. The nanoparticles, synthesized by co-precipitation, were extensively characterized by X-ray diffraction analysis, Brunauer–Emmett–Teller analysis and zeta potential analysis. The size and morphology of the particles were determined by scanning electron microscopy, which revealed an average particle size of ~130 nm. The synthesized nanoparticles were stable for at least 4 h in static conditions as evidenced by particle size measurements. Batch sorption studies were carried out, and sorption isotherms and reaction kinetics were analyzed. The iron oxide nanoparticles were not effective in fluoride removal at the pH and concentrations studied. They followed the Freundlich isotherm model and fitted well with pseudo-first-order reaction for As(III) and As(V) with R^2 value of 0.93 and 0.98 at pH 7, respectively. The maximum sorption capacity of the nanoparticles for As(III) and As(V) at pH 7 were 909 and 3,333 μg/g, respectively. The results of the study showed that the synthesized nanoparticles can be promising adsorbents for As removal in small-scale water systems.

Keywords: Iron oxide; Nanoparticles; Adsorption; Arsenic; Fluoride

1. Introduction

Access to safe drinking water is a vital indicator of a country's development and also a major prerequisite for a healthy life [1]. Recent WHO reports have estimated that about 663 million people do not have access to improved/safe water [2]. Thus, one of the Sustainable Development Goals (SDG 6) of the United Nations is to achieve universal access to safe and affordable drinking water for all by 2030 [3].

Groundwater is extensively used for drinking water supply particularly in the developing nations. However, groundwater may contain numerous inorganic anions and oxyanions due to natural and anthropogenic activities and may pose adverse health impacts [4,5]. Among the various inorganic pollutants, arsenic and fluoride have been determined to be major contaminants detrimental to human health [6].

Fluoride (F) is an essential element for dental health; however, prolonged consumption of water with elevated levels of fluoride (>1.5 mg/L) is detrimental to human health causing dental and skeletal fluorosis [7]. The common forms of arsenic species in environmental waters are arsenate (in oxidized waters) and arsenite (in reduced waters) [8]. Arsenic (As) is known to easily deposit in organs upon consumption of arsenic-rich water, and crops grown on arsenic accumulated soil cause arsenicosis [9]. Hence, in view of their adverse health impact, WHO has recommended maximum permissible limits of F and As as 1.5 mg/L and 10 μg/L, respectively [10]. However, potable water in many parts of China, India, Bangladesh, Central Africa and South America exceed the permissible limits of these contaminants, and hence, there is an urgent need to effectively remove As and F [11].

* Corresponding author.

Some of the commonly used defluoridation and arsenic removal methods are membrane filtration, ion exchange, chemical oxidation, chemical precipitation, electrolysis and coagulation [12]. However, most of these methods are limited by high-cost, pre- and post-treatment process and high pollutant concentrations of the water to be treated [12,13]. Among the various methods, adsorption offers potential advantages particularly in places where water is scarce and small-scale community-level or household-level water treatment is required. The process is also less energy intensive and offers other advantages like ease of operation, flexibility, simplicity of design and cost effectiveness [14,15].

Various materials have been tested as possible adsorbents for the removal of arsenic and fluoride from water, like alumina, iron-based oxides, rare metal oxides, activated carbon, bone char to name a few [16,17]. In recent decades, there has been increased interest in the application of nanomaterials in environmental applications such as in contaminant removal or toxicity mitigation [18]. Use of nanoparticles for pollutant removal is advantageous in view of their high reactivity and high surface area to volume ratio [19].

Among the various nanoparticles, magnetic nanoparticles are of particular interest in view of their high removal capacity, faster kinetics and most importantly magnetism [19] thereby minimising and simplifying post-separation process. The removal of the adsorbent with external magnetic field post-treatment is more selective and efficient than centrifugation or filtration [20]. A mixture of magnetite–maghemite nanoparticles have been effectively used for arsenic removal with a maximum adsorption of ~3.7 mg/g of As(III) and As(V) at pH 2 when the initial concentration of As was 1.5 mg/L [21]. Iron oxide nanoparticles immobilized in sodium alginate matrix have been studied for their fluoride removal potential. These nanoparticles exhibited a maximum adsorption capacity of ~58 mg/g of F for an initial concentration of 40 mg/L of F at pH 5 [22]. A number of F and As adsorption studies have shown maximum adsorption capacity at acidic pH. However, the pH of ground water is in the range of near neutral pH. Therefore, selecting an adsorbent, which demonstrates maximum adsorption capacity at near neutral pH, is crucial. In places with endemic fluoride and arsenic contamination in groundwater, fabrication and application of a suitable nanoadsorbent with simultaneous fluoride and arsenic removal potential would go a long way in reducing treatment cost when used in household-level water treatment.

Thus, the objectives of the present study were to elucidate the arsenic removal and defluoridation profile of iron oxide nanoparticles. In order to achieve this, iron oxide nanoparticles were synthesized and characterized, and their arsenic and fluoride removal efficiency at near neutral pH were studied. Additionally, adsorption isotherms were fitted to the experimental results, and kinetics of the sorption process were analyzed.

2. Materials and methods

2.1. Chemicals

Iron(III) chloride hexahydrate and iron(II) chloride tetrahydrate were procured from Merck KGaA, Germany. Sodium fluoride (J.T. Baker, Holland) was used to prepare standard fluoride solutions while $NaAsO_2$ and $NaAsO_4.12H_2O$ were used as sources of As(III) and As(V), respectively. All chemicals were of analytical grade and were used without further purification. Deionized water from Milli-Q was used throughout the experiments.

2.2. Preparation of iron oxide (Fe_3O_4) nanoparticles

The magnetic nanoparticles were prepared by a chemical co-precipitation method [23] with modifications. Briefly, 0.279 g of $FeCl_3.6H_2O$ and 1.395 g of $FeCl_2.4H_2O$ were dissolved in 100 mL ethanol so that the total molar concentration of Fe was 0.08 M. The experiment was performed under N_2 conditions, and 14.7 M NH_3 was added dropwise while stirring till the pH reached 9. Agitation was further continued for 5 min, and the flask was placed at 50°C for 3 h while stirring. Thereafter, the contents were transferred to centrifuge tubes and centrifuged at 10,000 rpm for 10 min. The pellet was washed thrice till the pH of supernatant became neutral and was further dried at 100°C for an additional 3 h.

The dried particles were then characterized and used for further studies.

2.3. Physicochemical characterization

2.3.1. X-ray diffraction (XRD) analysis

Preliminary characterization of the nanoparticles was performed using an XRD diffractometer (PANalytical-X'PERT PRO diffractometer system, Eindhoven, Netherlands). The target was Cu Kα with a wavelength of 1.54060 Å. The generator was operated at 40 kV and with a 300-mA current. The scanning range was selected between 10° and 100°. The crystallite size was also determined using the Debye–Scherrer equation.

2.3.2. Brunauer–Emmett–Teller (BET) and Barrett-Joyner-Halenda (BJH) analyses

The pore size, specific surface area, pore volume and pore size distribution of the synthesized nanoparticles were determined using BET surface area analyzer (Micromeritics Tri Star III, USA). The samples placed in sample cells were degassed and heated to 300°C for 2 h and cooled down to room temperature to remove moisture prior to analysis. The adsorption–desorption plots were used to calculate the specific surface area (N_2/BET method) and pore diameter. The pore volume and average pore size distribution was calculated based on summing through the pore size distribution, which is subjected to BJH model. This method is based on the assumption that the initial relative pressure is close to unity and all pores are filled with liquid.

2.3.3. Particle size analysis

The particle size range of the nanoparticles along with its polydispersity was determined using a particle size analyzer (Zetasizer Nano ZS, Malvern Instruments Ltd., UK). The average particle size was determined based on the hydrodynamic diameter (*z*-average) measured from the

autocorrelation function of the intensity of light scattered by the particles undergoing Brownian movement. The particles were dispersed in deionized water prior to analysis.

2.3.4. Zeta potential analysis

The surface electrostatic potential of the particles was determined using a zeta potential analyzer (Zetasizer Nano ZS, Malvern Instruments Ltd., UK). The particles were dispersed in 10^{-3} M KCl as a background electrolyte prior to measurement. About 3 mL of sample was used for analysis. Measurement was performed at various pH to determine the point of zero charge (PZC) of the particles. pH was adjusted using NaOH and HCl to prepare nanoparticles in the range of pH 3–10.

2.3.5. Scanning electron microscopy–energy-dispersive analysis X-ray spectroscopy (SEM–EDAX)

The surface morphology of the particles was determined using SEM (JSM-6010LA, JEOL USA Inc., USA), and the particles were dispersed in deionized water. The dispersed particles were then directly coated onto carbon tape and dried in a hot air oven prior to analysis. The elemental compositions of the nanoparticles were determined using SEM–EDAX.

The distribution of the nanoparticles were further analyzed using ImageJ version 1.51c, an open-source, Java-based imaging program [24,25].

2.3.6. Particle stability

The stability of the synthesized particles over time was determined by measuring the difference in particle size. The solution containing nanoparticles was left undisturbed, and sampling was done at different time points using a particle size analyzer.

2.4. Batch adsorption studies

2.4.1. Arsenic

Effect of As(III) and As(V) concentration on adsorption by synthesized iron oxide nanoparticles was determined by adding 0.05 g of nanoparticles in 50 mL of different concentrations of arsenic namely 100, 200, 400, 500 and 1,000 μg/L, respectively. Studies were carried out at pH 7. The bottles were continuously shaken at 180 rpm (Innova 2100 Platform Shaker, New Brunswick Scientific, USA) for 4 h at room temperature (20°C).

2.4.1.1. Chemical analysis

Samples were withdrawn at specific points in time and filtered through a 0.45-μm filter. Post filtration, the samples were diluted and acidified with concentrated nitric acid before analyzed using an atomic absorption spectrophotometer–graphite furnace (AAS–GF; solar thermo elemental with FS95 graphite furnace with autosampler) with a detection limit of 2 μg/L.

2.4.2. Fluoride

Similarly, the effect of fluoride concentration on adsorption by synthesized iron oxide nanoparticles was determined by adding 0.05 g of nanoparticles in 50 mL of different concentrations of fluoride namely 1, 3, 5, 7 and 10 mg/L at pH 7.

2.4.2.1. Chemical analysis

The filtered samples withdrawn at specific points in time was added in equal volume to TISAB III buffer (to release any complexed fluoride ions) before measurement using a fluoride ion selective electrode (WTW F 800 DIN, Germany).

The adsorption capacity was estimated by Eq. (1) as follows:

$$q_e = \frac{(C_o - C_e)V}{m} \quad (1)$$

The percentage adsorption was determined using the following equation:

$$\text{Adsorption efficiency}(\%) = \frac{(C_o - C_e)}{C_o} \times 100 \quad (2)$$

where q_e is the adsorption capacity (mg/g); C_0 and C_e are the initial and equilibrium concentration (μg/L and mg/L for As(III) and As(V), and F, respectively) of the contaminant, respectively; V is the volume of As and F solution (L) and m is the mass of the iron oxide nanoparticle (g).

2.4.3. Adsorption isotherms

Adsorption isotherms were obtained by batch equilibration technique. Isotherm experiments were performed at different pH values namely 6.5, 7 and 7.5 with varying concentrations of As(III), As(V) and F as mentioned in the previous section. Langmuir and Freundlich isotherms were used to fit the adsorption data from equilibrium experiments. The mechanism of adsorption process was tested by fitting the equilibrium data with the Dubinin–Radushkevich isotherm model (D–R isotherm).

2.4.4. Adsorption kinetics

The sorption capacity and percentage sorption of As(III), As(V) and F as a function of the equilibration time were determined by performing a study for equilibration periods (15 min–4 h). The concentrations of As(III) and As(V) selected for the study were 500 μg/L at pH 7. The data obtained was then plotted to determine the best fitting kinetic model to the data.

All the experiments were performed in duplicate in order to check reproducibility, and average values were used in the graphs.

3. Results and discussion

3.1. Synthesis of iron oxide nanoparticles

In the current study, a chemical co-precipitation method was used to synthesize iron oxide nanoparticles. The initial pH of the Fe^{2+} and Fe^{3+} solution in ethanol was 2.50, and the pH was observed to increase with a change in colour to black upon dropwise addition of NH_3 signalling the formation of iron oxide nanoparticles. The dried particles obtained were characterized further.

3.1.1. Characterization of synthesized iron oxide nanoparticles

3.1.1.1. XRD analysis Fig. 1 shows the XRD pattern of the iron oxide nanoparticles with distinct peaks at 30°, 35°, 43°, 57° and 63°, which corresponds to (220), (311), (400), (511) and (440) planes, respectively. The pattern did not show typical γ-Fe_2O_3 peaks corresponding to (210), (300) and (320) planes implying that the sample consisted of Fe_3O_4 magnetite nanoparticles [26]. Previous XRD studies on Fe_3O_4 nanoparticles synthesized by a similar co-precipitation method showed peaks corresponding to the same planes as observed in Fig. 1 [23]. XRD analysis thus confirmed the crystalline structure of the nanoparticles.

3.1.1.2. BET analysis In order to estimate the porosity of the synthesized nanoparticles, BET surface area analysis and BJH pore size and volume analysis were conducted. The surface area was found to be 75.24 $m^2 g^{-1}$ with a total pore volume of 0.018 $cm^3 g^{-1}$. The average pore size was calculated to be 1.1 nm. Increased number and size of the surface pores indicate an enhanced surface area [27,28], which is essential for adsorption applications. Related studies on the specific surface area of Fe_3O_4 nanoparticles prepared by chemical co-precipitation method yielded a surface area of 15.63 $m^2 g^{-1}$ [20].

3.1.1.3. Particle size analysis Particles of around 192 ± 5.96 nm in diameter were observed as seen from particle size analysis studies. The particles had a narrow size range with a polydispersity of 0.376. Thus, particle size analysis revealed the synthesis of nearly monodisperse particles with low polydispersity. Similar studies on the synthesis of Fe_3O_4 nanoparticles immobilized on sodium alginate matrix yielded a particle size ~140 nm [22].

3.1.1.4. Zeta potential analysis In order to determine the optimum pH for carrying out the batch sorption studies, a preliminary study to determine the effect of pH on the stability of the nanoparticles was carried out. The pH of the aqueous solution plays a major role in determining the surface charge of the adsorbent thereby also determining the adsorption performance [29]. Fig. 2 shows the PZC of the synthesized nanoparticles to be pH ~9. A decrease in surface zeta potential was observed with a corresponding increase in pH. The zeta potential was observed to be 0 at pH ~9 indicating that the particles were least stable at that pH. Contaminant removal studies were carried out at neutral pH (pH 7), and the surface zeta potential was approximately +60 mV indicating that the particles were highly stable at this pH. Iron oxide nanoparticles with a positive zeta potential value at low pH were also studied by Schwegmann et al. [30], and PZC at pH ~7 was obtained in their study. The zeta potential results thus suggested that the positively charged nanoparticles could be effectively used for the removal of negative ions.

3.1.1.5. SEM–EDAX studies Fig. 3(a) shows the SEM image of synthesized nanoparticles dispersed in aqueous solution. Monodisperse nearly spherical particles were observed from the image. EDAX analysis confirmed the presence of iron (Fe) in the samples (Fig. 3(b)). Table 1 shows the elemental composition of the particles. The presence of carbon (C) in the samples were due to mounting of the samples on carbon tape. ImageJ analysis of the SEM micrograph revealed the average particle size distribution to be 131 ± 4.87 nm. The difference in the particle size as revealed by SEM and dynamic light scattering (DLS) studies may have been due to the differences in the sample preparation [31]. The increased particle size in DLS could be due to various sources of attraction in the solution such as van der Waals forces of attraction.

3.1.1.6. Stability of nanoparticles The stability of the synthesized nanoparticles were also studied by measuring the change in particle size over a period of 24 h under static conditions. The results of the study are shown in Fig. 4. There was no significant change in particle size over a period of 4 h. At the end of 24 h, the particle size decreased by ~25 nm signifying settling down of larger particles. The results from the study indicated that the synthesized nanoparticles were stable for 4 h under static conditions. The characterized nanoparticles were then subsequently applied for batch sorption studies.

3.2. Batch sorption studies

Parameters like pH, adsorbent dosage, temperature and contact time were taken into account to optimize the system.

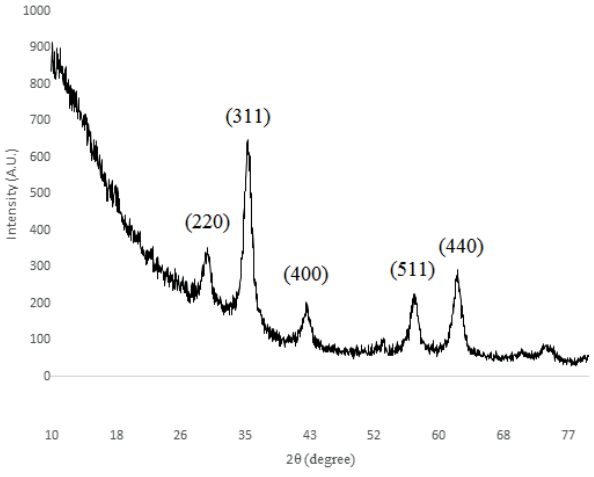

Fig. 1. XRD pattern of synthesized Fe_3O_4 nanoparticles.

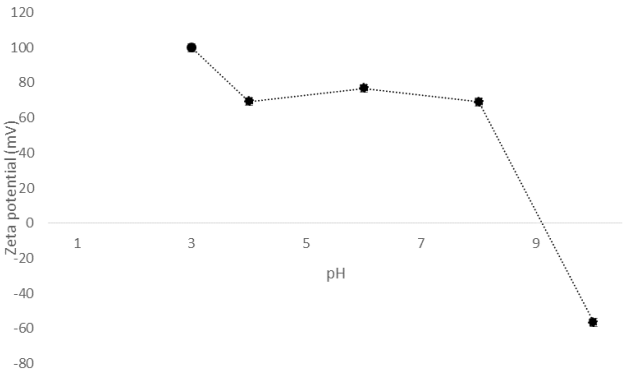

Fig. 2. Change in zeta potential of synthesized Fe_3O_4 nanoparticles vs. pH.

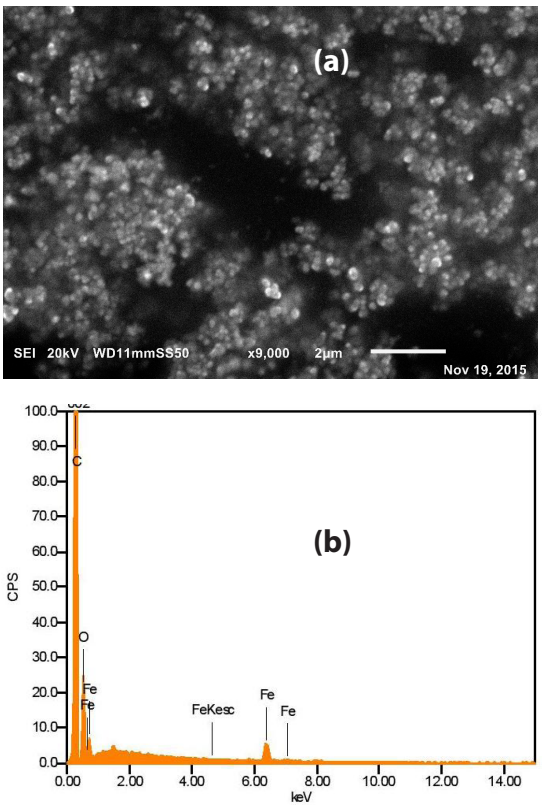

Fig. 3. SEM micrograph (a) and EDAX analysis (b) of synthesized Fe_3O_4 nanoparticles.

Table 1
Elemental composition of synthesized Fe_3O_4 nanoparticles

Element	Mass (%)
C	83.57
O	14.59
Fe	1.84

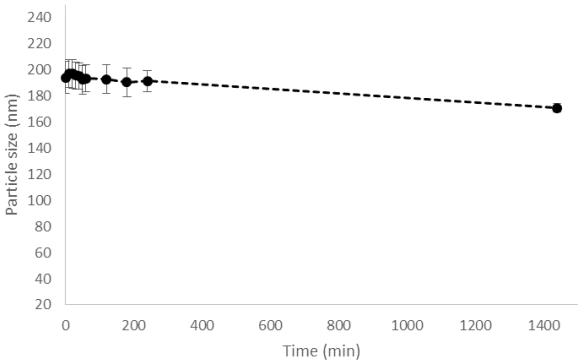

Fig. 4. Stability study of synthesized Fe3O4 nanoparticles.

For the optimized process of As batch adsorption studies, 0.05 g of iron oxide nanoparticles were added to 50 mL of 500 µg/L of As(III) and As(V) at pH 7 and interacted for 4 h at room temperature (20°C) while for the fluoride batch adsorption studies, the initial concentration of fluoride was 5 mg/L. Fig. 5 shows the schematic for the process of adsorption of fluoride and arsenic using iron oxide nanoparticles.

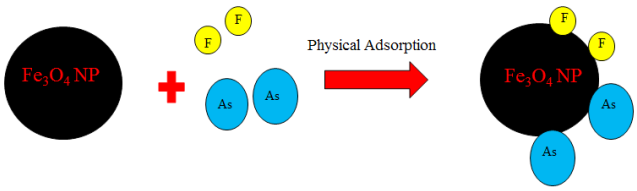

Fig. 5. Schematic showing physisorption of As and F ions by iron oxide nanoparticles.

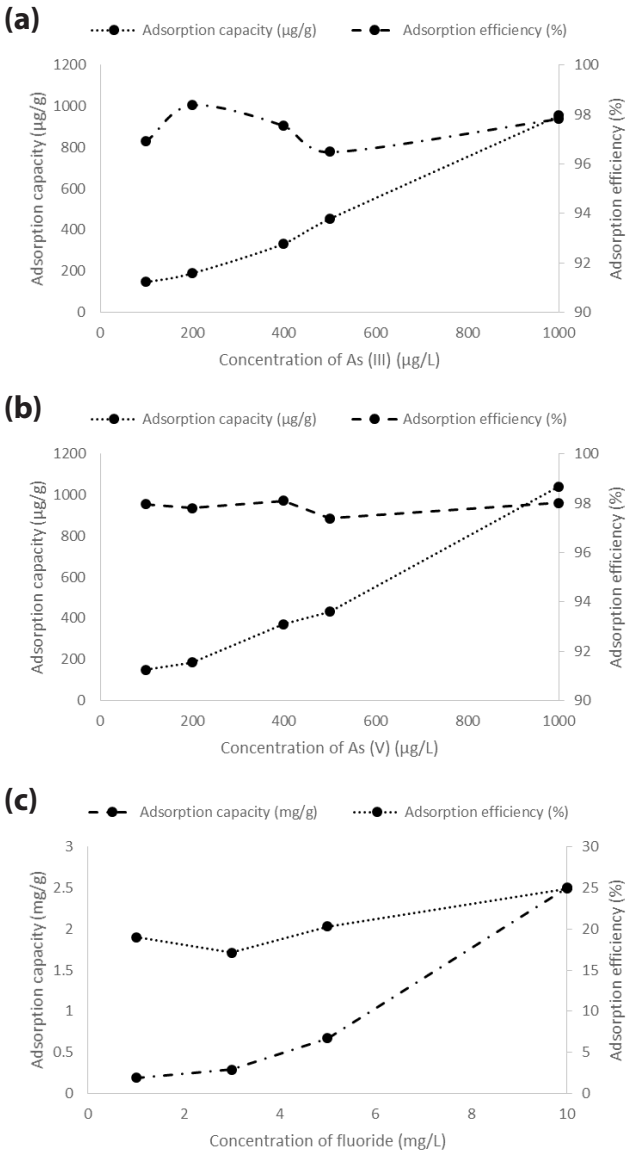

Fig. 6. Adsorption capacity and percentage adsorption of Fe_3O_4 nanoparticles as a function of: (a) As(III) concentration, (b) As(V) concentration and (c) F concentration (pH = 7.0, shaking speed = 180 rpm, temperature = 20°C).

3.2.1. Arsenic

3.2.1.1. Effect of initial As(III) and As(V) concentration The effect of As concentration on the adsorption efficacy of Fe_3O_4 nanoparticles was investigated in the current study. Figs. 6(a) and (b) shows the adsorption efficiency (%) and adsorption capacity (q_e) of iron oxide nanoparticles as a function of As(III) and As(V) concentration, respectively. In both cases, the adsorption capacity (q_e) was observed to increase with a corresponding increase in the As(III) and As(V) concentration, respectively. In general, the adsorption capacity (q_e) was higher for As(V) compared with As(III). As(V) is predominantly found in aerobic environments while As(III) predominates in moderately reducing anaerobic environments [32]. As(III) is considered more toxic than As(V), and As(III) is generally oxidized to As(V) before adsorption. Previous studies on superparamagnetic Fe_3O_4 nanoparticles capped by ascorbic acid with a particle size of ~10 nm had an adsorption capacity of 16.56 mg/g for As(V) and 46.06 mg/g for As(III), respectively [20]. The adsorption capacity largely depends on the particle size as smaller nanoparticles ensure larger surface area for adsorption. Increased surface area as evidenced by BET analysis indicates an increased number of favourable sites for adsorption.

3.2.2. Fluoride

3.2.2.1. Effect of initial fluoride concentration Fig. 6(c) shows the effect of initial F concentration on adsorption efficiency (%) and adsorption capacity (mg/g) of the synthesized Fe_3O_4 nanoparticles. Increase in the initial F concentration led to a corresponding increase in the adsorption capacity of Fe_3O_4 nanoparticles. The maximum percentage adsorption was achieved when the initial F concentration was 10 mg/L (~25%). The amount of F adsorbed at pH 6.5 (1.78 mg/g) was approximately 10 times lower as compared with studies carried out using polypyrrole/Fe_3O_4 nanocomposites (17.6 mg/g) [33]. Hence, the synthesized Fe_3O_4 nanoparticles may not be a suitable adsorbent under the conditions applied in this study for fluoride adsorption in the absence of surface modification.

3.3. Isotherm studies

In order to further determine the mode of adsorption of the adsorbent, isotherm studies were carried out, and the data was analyzed. Among the various models, Langmuir and Freundlich are the ones most frequently used for adsorption studies [29].

The Langmuir isotherm model assumes that adsorption takes place by monolayer sorption and also assumes that the adsorption sites are energetically the same [34]:

$$\frac{C_e}{q_e} = \frac{1}{q_m} C_e + \frac{1}{k_\alpha q_m} \quad (3)$$

while the Freundlich model is an empirical description of adsorption on a heterogeneous surface [35]:

$$\log q_e = \log k_f + \frac{1}{n} \log C_e \quad (4)$$

Table 2
Summary of parameters obtained from Langmuir and Freundlich isotherms for As(III) adsorption by Fe_3O_4 nanoparticles

pH	Freundlich model			Langmuir model		
	k_f (μg/g)	1/*n*	R^2	q_m (μg/g)	k_α	R^2
6.5	17.34	0.85	0.88	909.1	0.02	0.87
7	25.35	1.12	0.93	909.1	0.06	0.68
7.5	21.65	0.75	0.98	714.28	0.02	0.99

Table 3
Summary of parameters obtained from Langmuir and Freundlich isotherms for As(V) adsorption by Fe_3O_4 nanoparticles

pH	Freundlich model			Langmuir model		
	k_f (μg/g)	1/*n*	R^2	q_m (μg/g)	k_α	R^2
6.5	25.03	0.88	0.97	3,333.3	0.01	1
7	46.88	0.99	0.98	3,333.3	0.02	0.98
7.5	72.7	0.96	0.77	1,000	0.05	0.62

where q_e is the amount of sorbate adsorbed at equilibrium per g of Fe_3O_4 nanoparticles; C_e is the concentration of sorbate at equilibrium; q_m is monolayer sorption capacity (mg/g); k_α is the Langmuir sorption equilibrium constant and k_f and 1/*n* are the Freundlich constants.

3.3.1. Arsenic

Tables 2 and 3 show a summary of parameters obtained from Langmuir and Freundlich isotherms for As(III) and As(V) adsorption by Fe_3O_4 nanoparticles at different pH values 6.5, 7 and 7.5. Tables 2 and 3 indicated a decrease in the q_m value with increase in pH. The lowest q_m value (mg/g) was observed at pH 7.5. The decrease was possibly due to the changes in the zeta potential of the nanoparticles with change in pH. The net positive charge on the surface of nanoparticles decreased with increase in pH thereby leading to less favourable adsorption of As(III) and As(V) at pH 7.5. The results are in accordance with previous studies on ascorbic acid coated Fe_3O_4 particles for As(III) and As(V) adsorption. A 15% decrease in As(III) and As(V) removal percentage was observed in this case upon increase in pH above 7 [20]. Comparing the q_m values between As(III) and As(V) showed that Fe_3O_4 nanoparticles had ~3 times more adsorption capacity for As(V) than As(III), suggesting that Fe_3O_4 nanoparticles had higher sorption capacity for As(V) than As(III). The Freundlich equilibrium isotherm equation gave relatively better description of sorption of As(V) (R^2 value = 0.98) and As(III) (R^2 value = 0.93).

Han et al. [36] reported the As(III) adsorptive capacity of iron-oxide-coated rock to be 1.65 mg/g, and the system followed the Langmuir isotherm. α-Fe_2O_3 nanoparticles have also been studied for their As(III) and As(V) removal capacity. Adsorption capacities of 95 and 47 mg/g for As(III) and As(V), respectively, were obtained from the study [37]. The results from the current study were significantly higher than the adsorption capacity of commercial iron oxide samples (0.46 mg/g) [38].

Table 4
Summary of parameters obtained from Langmuir and Freundlich isotherms for fluoride adsorption by Fe_3O_4 nanoparticles

pH	Freundlich model			Langmuir model		
	k_f (mg/g)	1/*n*	R^2	q_m (mg/g)	k_α	R^2
6.5	0.59	0.63	0.73	1.78	0.64	0.76
7	0.78	0.45	0.64	1.47	1.78	0.48
7.5	0.54	0.42	0.55	1.20	1.22	0.70

3.3.2. Fluoride

Table 4 shows the Langmuir and Freundlich isotherm parameters for fluoride adsorption by Fe_3O_4 nanoparticles. A steady decrease in the q_m (mg/g) values was observed with a corresponding increase in the pH. On comparison with the results from Table 3, it could be noted that the adsorption capacity of the nanoparticles was highest for As(V).

3.3.3. D–R isotherm

The D–R isotherm model is used to predict the sorption nature of the adsorbate on adsorbent, and the linear form of the equation may be written as follows [39]:

$$\ln q_e = \ln q_s - K^2 \tag{5}$$

$$\varepsilon = RT \ln\left(1 + \frac{1}{C_e}\right) \tag{6}$$

where ε is the Polanyi potential; *R* is the gas constant (J /mol K); *T* is the absolute temperature (K); C_e is the equilibrium concentration of contaminant in aqueous solution (g/L); q_e is the amount of contaminant adsorbed per unit weight of iron oxide nanoparticles (g/g) and q_s is the adsorption capacity (g/g).

The D–R isotherm constant *K* can be calculated from the slope of the plot of $\ln q_e$ against ε^2. The mean free energy of adsorption, *E*, was then calculated from the obtained *K* value:

$$E = (-2K)^{-0.5} \tag{7}$$

If *E* is in the range between 8 and 16 kJ/mol, the reaction is due to chemisorption. However, if the value of *E* < 8 kJ/mol, the reaction is purely physisorption. The mean free energy of adsorption in our study was found to be 5.8, 5.85 and 7.68 kJ/mol at pH 7 for As(III), As(V) and F, respectively, implying that physisorption took place in all the cases.

It is to be noted that the adsorption capacity of Fe_3O_4 nanoparticles presented here is based on the study with model groundwater. In the presence of other common groundwater ions, the adsorption capacity would be different. Depending on the type of ions (charge, molecular weight, solubility etc.) present, the capacity may possibly either increase, remain the same or even increase [40]. For example, increasing concentration of phosphate (0.5–5 mg/L) in spiked groundwater samples was found to decrease arsenic adsorption (from 88% to 60%) by magnetite–maghemite nanoparticles [21]. Cations such as Ca and Mg in groundwater have been found to have synergistic effect on As(V) adsorption by TiO_2 nanoparticles due to electrostatic attraction, while exhibiting negligible effects towards As(III) [41].

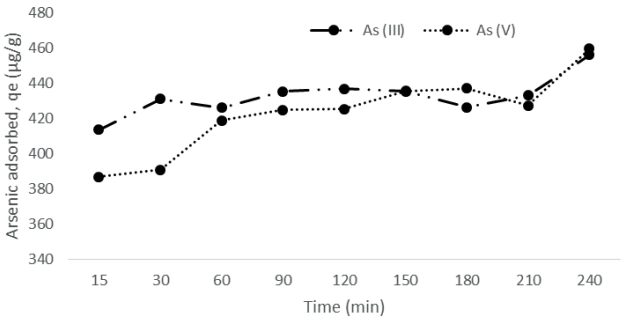

Fig. 7. Short-term kinetics of arsenic adsorption as a function of time (pH = 7.0, concentration = 500 µg/L, shaking speed = 180 rpm, temperature = 20°C).

3.4. Adsorption kinetics

A study was also carried out to determine the kinetics of sorbate adsorbed within the equilibration time. The change in As(III) and As(V) adsorbed within the equilibration time is shown in Fig. 7. The results obtained were in accordance with the As(III) and As(V) adsorbed at the end of 4 h. The As(III) adsorbed increased from 413.65 µg/g in 15 min to 456.18 µg/g at the end of 4 h as compared with 386.81 µg/g in 15 min to 459.82 µg/g in 4 h for As(V). Similarly, the 4 h results of fluoride adsorbed from the short-term kinetics studies were in accordance with the results of the batch sorption study.

The next part of the study was to determine the kinetic model best fitting the data. Adsorption kinetic parameters are important in predicting adsorption rate and also in designing adsorption-based water treatment systems [42]. The rate at which the sorbate gets adsorbed onto the Fe_3O_4 nanoparticles can be determined using the rate-order kinetics.

The pseudo-first-order reaction can be written as [43]:

$$\log(q_e - q_t) = \log q_e - \left(\frac{k_1}{2.303}\right)t \tag{8}$$

while the pseudo-second-order reaction may be written as [44]:

$$1/(q_e - q_t) = (1/q_e) + k_2 t \tag{9}$$

where q_e and q_t are the fluoride and arsenic adsorbed at equilibrium and at time *t*, respectively, and k_1 and k_2 are the rate constants of the pseudo-first-order and pseudo-second-order reaction, respectively.

Fig. 8 plots the pseudo-first-order kinetic modelling plot of $\log(q_e - q_t)$ vs. *t* for As(III) and As(V). The pseudo-first-order parameters were a better fit with the data than the pseudo-second-order parameters. Compared with As(III), As(V) had a better fit to the pseudo-first-order model as indicated by the correlation coefficient values. The rate constant k_1 values of 0.003 and 0.005 was calculated for As(III) and As(V), respectively, while the corresponding pseudo-second-order

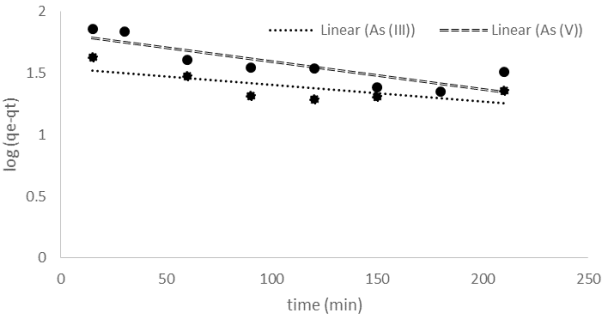

Fig. 8. Pseudo-first-order kinetic modelling plot of $\log(q_e - q_t)$ vs. time for As(III) and As(V) (pH = 7.0, concentration = 500 μg/L, shaking speed = 180 rpm, temperature = 20°C).

Table 5
Summary of pseudo-first-order and pseudo-second-order reaction constants for As(III) and As(V) under optimized conditions

Type	k_1 (min)	R^2	k_2 (min)	R^2
As(III)	0.003	0.52	0.0001	0.48
As(V)	0.005	0.74	0.0001	0.72

rate constants were 0.0001 for both As(III) and As(V). Table 5 summarizes the calculated parameters fitting the pseudo-first-order and pseudo-second-order reactions.

In summary, iron oxide nanoparticles, which were synthesized using a chemical co-precipitation method, were effective adsorbents for both As(III) and As(V). The nanoparticles exhibited an adsorption capacity of ~1,000 μg/g at As concentration of 1,000 μg/L, pH 7. Effect of parameters like pH and initial concentration of As were studied for their effect on the removal. Increase in adsorption capacity was observed with increase in initial concentration, and the particles followed Freundlich model of adsorption. The particles followed pseudo-first-order kinetics for both As(III) and As(V). Further studies may be focussed on determining the effect of other parameters like presence of other anions, temperature and concentration of the nanoparticle etc. on the adsorption process. In the case of fluoride, the nanoparticles did not exhibit significant removal at different concentrations of fluoride and at different pH. The removal was not comparable with those cited in the literature. Further modifications on the nanoparticles, like surface coating with alumina, may be required to improve its efficiency for fluoride removal.

4. Conclusions

- The present study demonstrated the application of unmodified Fe_3O_4 nanoparticles for effective removal of arsenic and fluoride from aqueous solutions.
- The removal of arsenic and fluoride from the contaminated waters depends on parameters like pH, initial concentration of arsenic and fluoride, and also interaction time. There was no significant removal efficiency of fluoride from the aqueous solution using Fe_3O_4 nanoparticles.
- The synthesized nanoparticles had significant adsorption efficiency for As(III) (~97%) and As(V) (~98%) at pH 7 and at a As concentration of 1,000 μg/L.
- The nanoparticles followed the Freundlich model of adsorption, and the kinetic data fitted the pseudo-first-order reaction kinetics with k_1 values of 0.003 and 0.005 for As(III) and As(V), respectively. The D–R isotherm fitting revealed that adsorption process was physisorption.
- Further detailed studies would be required to provide insight into the various factors affecting the adsorption of As(III) and As(V) by synthesized iron oxide nanoparticles.
- The iron oxide nanoparticles did not demonstrate significant adsorption of fluoride at the concentrations studied as compared with other available adsorbents for fluoride. Functionalization of the iron oxide nanoparticles to form iron/alumina nanocomposites may be performed to determine its enhanced efficacy, if any, towards fluoride adsorption.

Acknowledgements

This study was carried out as a part of EU COFUND project – Experienced Water Postdoc Fellowship (Grant Agreement No. 606838). The authors are thankful to Prof. Amitava Mukherjee (VIT University) and Mr. Rajeev Mudakavi (Indian Institute of Science) for help with BET and XRD analysis and also acknowledge the support of UNESCO-IHE lab staff in conducting various analysis.

References

[1] J. Fawell, M. Nieuwenhuijsen, Contaminants in drinking water, Br. Med. Bull., 68 (2003) 199–208.
[2] WHO/UNICEF, Progress on Sanitation and Drinking-water – 2015 Update and MDG Assessment, Joint Monitoring Programme: World Health Organization and United Nations Children Education Fund, 2015, p. 1.
[3] United Nations, Transforming Our World: The 2030 Agenda for Sustainable Development, A/RES/70/1, 2015.
[4] N.A. Oladoja, S. Hu, J.E. Drewes, B. Helmreich, Insight into the defluoridation efficiency of nano magnesium oxide in groundwater system contaminated with hexavalent chromium and fluoride, Sep. Purif. Technol., 162 (2016) 195–202.
[5] S.V. Jadhav, E. Bringas, G.D. Yadav, V.K. Rathod, I. Ortiz, K.V. Marathe, Arsenic and fluoride contaminated groundwaters: a review of current technologies for contaminants removal, J. Environ. Manage., 162 (2015) 306–325.
[6] T. Thompson, J. Fawell, S. Kunikane, D. Jackson, S. Appleyard, P. Callan, J. Bartram, P. Kingston, Chemical Safety of Drinking Water: Assessing Priorities for Risk Management, World Health Organization, Geneva, 2007.
[7] P. Miretzky, A.F. Cirelli, Fluoride removal from water by chitosan derivatives and composites: a review, J. Fluor. Chem., 132 (2011) 231–240.
[8] K.P. Raven, A. Jain, R.H. Loeppert, Arsenite and arsenate adsorption on ferrihydrite: kinetics, equilibrium and adsorption envelopes, Environ. Sci. Technol., 32 (1998) 344–349.
[9] Q. Guo, J. Tian, Removal of fluoride and arsenate from aqueous solution by hydrocalumite via precipitation and anion exchange, Chem. Eng. J., 231 (2013) 121–131.
[10] WHO, Guidelines for Drinking Water Quality, World Health Organization, Vol. 1, 2011, p. 178.
[11] A.L. Rose, T.D. Waite, Kinetic model for Fe(II) oxidation in seawater in the absence and presence of natural organic matter, Environ. Sci. Technol., 36 (2002) 433–444.
[12] Y. Tian, M. Wu, R. Liu, D. Wang, X. Lin, W. Liu, L. Ma, Y. Li, Y. Huang, Modified native cellulose fibres – a novel efficient adsorbent for both fluoride and arsenic, J. Hazard. Mater., 185 (2011) 93–100.

[13] R. Liu, W. Gong, H. Lan, T. Yang, H. Liu, J. Qu, Simultaneous removal of arsenate and fluoride by iron and aluminum binary oxide: competitive adsorption effects, Sep. Purif. Technol., 92 (2012) 100–105.
[14] V. Kumar, N. Talreja, D. Deva, N. Sankararamakrishnan, A. Sharma, N. Verma, Development of bi-metal doped micro- and nano multi-functional polymeric adsorbents for the removal of fluoride and arsenic(V) from wastewater, Desalination, 282 (2011) 27–38.
[15] M. Sarkar, A. Banerjee, P.P. Pramanick, A.R. Sarkar, Use of laterite for the removal of fluoride from contaminated drinking water, J. Colloid Interface Sci., 302 (2006) 432–441.
[16] E. Henden, T.D. Ciftci, Separation of Arsenic from Waters using Inorganic Adsorbents, M. Bryjak, N. Kabay, B.L. Rivas, B. Jochen, Eds., Innovative Materials and Methods for Water Treatment: Solutions for Arsenic and Chromium Removal, CRC Press, Leiden, 2016, pp. 67–78.
[17] M.H. Stanic, M.E. Ravancic, A. Flanagan, A review on adsorption of fluoride from aqueous solution, Materials, 7 (2014) 6317–6366.
[18] P.G. Tratnyek, R.L. Johnson, Nanotechnologies for environmental cleanup, Nano Today, 1 (2006) 44–48.
[19] S.C.N. Tang, I.M.C. Lo, Magnetic nanoparticles: essential factors for sustainable environmental applications, Water Res., 47 (2013) 2613–2632.
[20] L. Feng, M. Cao, X. Ma, Y. Zhu, C. Hu, Superparamagnetic high surface area Fe_3O_4 nanoparticles as adsorbents for arsenic removal, J. Hazard. Mater., 217–218 (2012) 439–446.
[21] S.R. Chowdhury, E.K. Yanful, Arsenic and chromium removal by mixed magnetite-maghemite nanoparticles and the effect of phosphate on removal, J. Environ. Manage., 91 (2010) 2238–2247.
[22] E. Christina, P. Viswanathan, Development of a novel nano-biosorbent for the removal of fluoride from water, Chin. J. Chem. Eng., 23 (2015) 924–933.
[23] C. Zhang, L. Chen, T.J. Wang, C.L. Su, Y. Jin, Synthesis and properties of a magnetic core–shell composite nano-adsorbent for fluoride removal from drinking water, Appl. Surf. Sci., 317 (2014) 552–559.
[24] M.D. Abramoff, P.J. Magalhaes, S.J. Ram, Image Processing with ImageJ, Biophoton. Int., 11 (2004) 36–42.
[25] ImageJ Software Version 1.51c, 2016. Available from: rsb.info.nih.gov-ij
[26] P. Velusamy, S.C. Hung, A. Shritama, S.G. Kumar, V. Jeyanthi, K. Pandian, Synthesis of oleic acid coated iron oxide nanoparticles and its role in anti-biofilm activity against clinical isolates of bacterial pathogens, J. Taiwan Inst. Chem. Eng., 59 (2016) 450–456.
[27] C. Gao, Y. Wan, C. Yang, K. Dai, T. Tang, H. Luo, J. Wang, Preparation and characterization of bacterial cellulose sponge with hierarchical pore structure as tissue engineering scaffold, J. Porous Mater., 18 (2011) 139–145.
[28] J. Guo, J.M. Catchmark, Surface area and porosity of acid hydrolyzed cellulose nanowhiskers and cellulose produced by *Gluconacetobacter xylinus*, Carbohydr. Polym., 87 (2012) 1026–1037.
[29] W. Li, C.Y. Cao, L.Y. Wu, M.F. Ge, W.G. Song, Superb fluoride and arsenic removal performance of highly ordered mesoporous aluminas, J. Hazard. Mater., 198 (2011) 143–150.
[30] H. Schwegmann, A.J. Feitz, F.H. Frimmel, Influence of the zeta potential on the sorption and toxicity of iron oxide nanoparticles on S. cerevisiae and E. coli, J. Colloid Interface Sci., 347 (2010) 43–48.
[31] T.C. Prathna, N. Chandrasekaran, A.M. Raichur, A. Mukherjee, Biomimetic synthesis of silver nanoparticles by Citrus limon (lemon) aqueous extract and theoretical prediction of particle size, Colloids Surf., B, 82 (2011) 152–159.
[32] D. Mohan, C.U. Pittmann Jr., Arsenic removal from water/wastewater using adsorbents—a critical review, J. Hazard. Mater., 142 (2007) 1–53.
[33] M. Bhaumika, T.Y. Leswifia, A. Maity, V.V. Srinivasu, M.S. Onyango, Removal of fluoride from aqueous solution by polypyrrole/Fe_3O_4 magnetic nanocomposite, J. Hazard. Mater., 186 (2011) 150–159.
[34] I. Langmuir, The constitution and fundamental properties of solid and liquids. Part I. Solids, J. Am. Chem. Soc., 38 (1916) 2221–2295.
[35] H. Freundlich, Tiber die adsorption in Losungen, Z. Phys. Chem., 57 (1906) 385–470.
[36] Y. Han, X. Wu, Y. Ma, L. Gong, F. Qu, H. Fan, Porous SnO_2 nanowire bundles for photocatalyst and Li ion battery applications, CrystEngComm, 13 (2011) 3506–3510.
[37] W. Tang, Q. Li, S. Gao, J.K. Shang, Arsenic (III,V) removal from aqueous solution by ultrafine ⌾-Fe_2O_3 nanoparticles synthesized from solvent thermal method, J. Hazard. Mater., 192 (2011) 131–138.
[38] L.S. Zhong, J.S. Hu, H.P. Liang, A.M. Cao, W.G. Song, L.J. Wan, Self-assembled 3D flowerlike iron oxide nanostructures and their application in water treatment, Adv. Mater., 18 (2006) 2426–2431.
[39] M.M. Dubinin, L.V. Radushkevich, Equation of the Characteristic Curve of Activated Charcoal, Proc. Academy of Sciences, Physical Chemistry Section, USSR, Vol. 55, 1947, pp. 331–333.
[40] L. Yan, S. Hu, C. Jing, Recent progress of arsenic adsorption on TiO_2 in the presence of coexisting ions: a review, J. Environ. Sci., 49 (2016) 74–85.
[41] J. Cui, J. Du, S. Yu, C. Jing, T. Chan, Groundwater arsenic removal using granular TiO_2: integrated laboratory and field study, Environ. Sci. Pollut. Res., 22 (2015) 8224–8234.
[42] R.I. Yousef, B. El-Eswed, A. Al-Muhtaseb, Adsorption characteristics of natural xeolites as solid adsorbents for phenol removal from aqueous solution: kinetics, mechanism and thermodynamic studies, Chem. Eng. J., 171 (2011) 1143–1149.
[43] S. Lagergren, About the theory of so-called adsorption of soluble substances, K. Sven. Vetenskapsakad. Handl., 24 (1898) 1–39.
[44] J. Wang, W. Xu, L. Chen, X. Huang, J. Liu, Preparation and evaluation of magnetic nanoparticles impregnated chitosan beads for arsenic removal from water, Chem. Eng. J., 251 (2014) 25–34.